MASTER COPY KEEP THIS COPY FOR REPRODUCTION PURPOSES

REPORT DOCUMENTATION PAGE

Form Approved
OMB No. 0704-0188

1. AGENCY USE ONLY (Leave blank)	2. REPORT DATE	3. REPORT TYPE AND DATES COVERED
	September 24, 1995	Final Report, 8/1/92 - 7/31/95

4. TITLE AND SUBTITLE
The Fluid Mechanics of Vortex Cutting By a Blade

5. FUNDING NUMBERS
DAAH04-93-G-0378

6. AUTHOR(S)
Jeffrey S. Marshall

7. PERFORMING ORGANIZATION NAME(S) AND ADDRESS(ES)
The University of Iowa
Iowa City, Iowa 52242

8. PERFORMING ORGANIZATION REPORT NUMBER

9. SPONSORING/MONITORING AGENCY NAME(S) AND ADDRESS(ES)
U. S. Army Research Office
P. O. Box 12211
Research Triangle Park, NC 27709-2211

10. SPONSORING/MONITORING AGENCY REPORT NUMBER
ARO 32300.7-EG-YIP

11. SUPPLEMENTARY NOTES
The view, opinions and/or findings contained in this report are those of the author(s) and should not be construed as an official Department of the Army position, policy, or decision, unless so designated by other documentation.

12a. DISTRIBUTION/AVAILABILITY STATEMENT
Approved for public release; distribution unlimited.

12b. DISTRIBUTION CODE

19951023 019

13. ABSTRACT (Maximum 200 words)

A study of the fluid dynamics associated with impact of a vortex on a body (such as a blade) moving normal to the vortex axis was performed. The physical features of the flow evolution were categorized in terms of two dimensionless parameters, which represent a ratio of length scales and a ratio of velocity scales associated with the vortex core and with the body. Models of various features of the flow evolution are constructed and compared against experimental and detailed computational data. Primary features of interest in the study include vortex deflection and axial flow in the vortex core resulting from stretching by the blade, intense vorticity deformation resulting from penetration of the body into the vortex core (and resulting force on the body), traveling vortex breakdown formed immediately following vortex cutting by the body, and interaction of shed vorticity from the body with the primary vortex.

14. SUBJECT TERMS			15. NUMBER OF PAGES
Vortex Cutting, Blade-Vortex Interaction, Helicopter Aerodynamics			33
			16. PRICE CODE
17. SECURITY CLASSIFICATION OF REPORT	18. SECURITY CLASSIFICATION	19. SECURITY CLASSIFICATION OF ABSTRACT	20. LIMITATION OF ABSTRACT
UNCLASSIFIED	UNCLASSIFIED	UNCLASSIFIED	UL

DISCLAIMER NOTICE

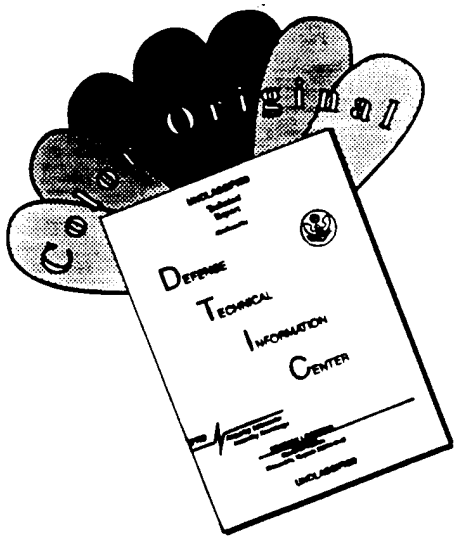

THIS DOCUMENT IS BEST QUALITY AVAILABLE. THE COPY FURNISHED TO DTIC CONTAINED A SIGNIFICANT NUMBER OF COLOR PAGES WHICH DO NOT REPRODUCE LEGIBLY ON BLACK AND WHITE MICROFICHE.

The Fluid Mechanics of Vortex Cutting By a Blade

Final Report

J.S. Marshall

September 30, 1995

U.S. Army Research Office
Grant Number DAAH04-93-G-0378

The University of Iowa

TABLE OF CONTENTS

Page

LIST OF FIGURES ii

1. Statement of the Problem 1

2. Summary of the Most Important Results 4

a.) Regimes of normal blade-vortex interaction 5
b.) Computations of blade penetration into a vortex core 14

3. Conclusions and future work 27

LIST OF PUBLICATIONS AND TECHNICAL REPORTS 29
LIST OF PARTICIPATING SCIENTIFIC PERSONNEL 31
REPORT OF INVENTIONS 31
BIBLIOGRAPHY 32

LIST OF FIGURES

Page

Fig. 1. Schematic of normal blade-vortex interaction 3

Fig. 2. Pictures showing secondary vortex wrapping about the primary vortex in the strong-vortex regime (regime 1) 7

Fig. 3. Computation of vortex bending about a circular cylinder in regime 3 10

Fig. 4. Computation vortex "shock" formed after cutting of vortex by blade 11

Fig. 5. Pictures of vortex breakdowns of the (a) bubble and (b) spiral types 12

Fig. 6. Perspective view of the initial configuration for the computations of blade penetration into a vortex core 15

Fig. 7. Plot of the variation with time of the computed values of circulation in the $y = 0$ plane as the vortex is penetrated by the blade for three nominal circulation values 18

Fig. 8. Side view of the vorticity field for a case with $\Gamma / 2\pi\sigma U = 1.6$ at time t=0.23 19

Fig. 9. Plot of average vorticity magnitude of the thirty control points with highest vorticity magnitude for direct computation, with three circulation values, in comparison with RDT results 20

Fig. 10. Contour plot of the pressure change on the blade surface due to the vortex for a case with $\Gamma / 2\pi\sigma_0 U = 1.6$ and at time $t = 0.26$ 22

Fig. 11. Plot of variation of the minimum value of the blade surface pressure coefficient $C_{p,\min}$ with time for cases with strong, moderate and weak vortices, in comparison to RDT results 24

Fig. 12. Plot of variation of the drag coefficient C_D with time for cases with strong, moderate and weak vortices, in comparison with RDT results (circles) 26

THE FLUID MECHANICS OF VORTEX CUTTING BY A BLADE

1. Statement of the Problem

The problem under consideration in this study involves the impingement of a vortex onto a blade, where the blade travels relative to the vortex in a direction normal to the vortex axis, as shown in figure 1. This problem will hereinafter be referred to as normal blade-vortex interaction (BVI). The primary application of this research is in the area of helicopter interactional aerodynamics. During the course of the research, the scope of the study has evolved such that we interpret the term "blade", in a loose manner, to be any body which is very long in one direction, oriented approximately normal to the vortex axis (see figure 1). The research would thus apply to problems involving interaction of helicopter main rotor vortices with the tail or empennage sections of the helicopter, which is a common occurrence in low speed flight, or (for some designs) with the tail rotor blades (Leverton et al., 1977). The research would also apply to problems such as ingestion of atmospheric turbulence or the helicopter "ground vortex" into the main rotor.

The results of this project have been reported in two parts, which respectively consider the nature of the vortex response to the blade as a function of the two dimensionless parameters, T/σ and $\Gamma/2\pi\sigma U$. The first of these parameters represents the ratio of the blade "thickness", T, to the ambient vortex core radius, σ, while the second parameter represents the ratio of the maximum nominal vortex swirl velocity, $\Gamma/2\pi\sigma$, to the blade speed, U, relative to the vortex axis. The effects of these parameters on the vortex flow is examined using a combination of experiment, numerical computation and analytical modeling.

The first part of the study, which has previously been reported to ARO (Marshall, 1993), concentrates primarily on the effect of T/σ on the vortex response. It is found that this parameter is primarily responsible for determining the amount that a vortex will bend, due to the inviscid interaction, as it comes close to the blade. Two basic regimes of interaction were identified, one for small T/σ, in which the vortex remains

approximately unbent as comes close to and is eventually cut by the blade, and one for large T/σ, in which the vortex undergoes a large displacement and wraps about the blade leading edge.

The second part of the research, reported here, is concerned with the effect of the second parameter, $\Gamma/2\pi\sigma U$, on the vortex response. In the context of an inviscid flow with small T/σ, so that the blade penetrates into the vortex, the combination $(T/\sigma)(\Gamma/2\pi\sigma U)$ is found to play a central role in determining whether the vortex deformation is due primarily to the vortex-induced flow or to the ambient potential flow past the blade. In the latter case, approximations such as rapid distortion theory (RDT) can be used to simplify calculation of the unsteady force on the blade, as is commonly done in models of sound generation from blade-vortex interaction (Howe, 1989, Amiet et al., 1990). For viscous flow, the parameter $\Gamma/2\pi\sigma U$ influences the time at which secondary vorticity is shed from the blade by the vortex-induced flow and the extent to which the shed vorticity influences the primary vortex prior to impinging on the blade.

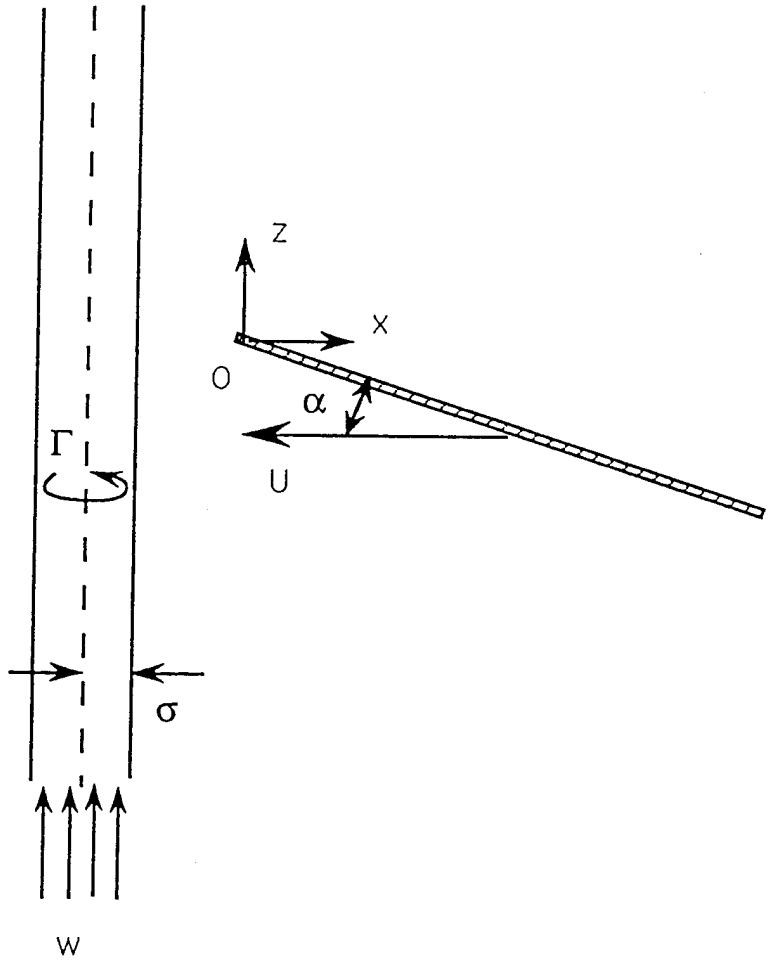

Fig. 1. Schematic of normal blade-vortex interaction, showing core axial flow w, vortex core radius σ, vortex circulation Γ, blade speed U and angle of attack α.

2. Summary of the Most Important Results

The simplest model of vortex-blade interaction is that of an infinitesimally thin vortex filament impinging on a blade of thickness T, where the vortex filament wraps around the blade and comes progressively closer to the blade surface as time advances. Let b denotes the minimum separation distance between the vortex filament and the blade surface. As the vortex filament comes very close to the surface the blade surface pressure would exhibit a $1/b^2$ singularity and the force exerted on the blade by the vortex would exhibit a $1/b$ singularity, thus becoming infinite as $b \to 0$. This singularity is clearly non-physical; it is an artifact of the assumption in the model that all of the vorticity is concentrated on a curve.

There are several ways in which the force singularity might be resolved. For instance, one might assume that the vortex core remains circular but has a finite radius which is uniform along the vortex (Affes and Conlisk, 1993). One might alternatively make allowance for the fact that the part of the vortex near the blade is stretched more rapidly than the part far from the blade by allowing the core radius of the filament to vary with position along the vortex axis, but then it is also necessary to account for the strong axial flow within the vortex that forms as a result of the gradient in core radius (Marshall and Yalamanchili, 1994). One might let the core shape deform from a circular shape, which would occur due to interaction with the vortex image (e.g., Saffman and Tanveer, 1982). For cases where the blade thickness is of the same order as or much thinner than the vortex core radius, the blade is observed to penetrate into the vortex core, in which case it is necessary to account for the very strong vorticity deformation occurring close to the leading edge of the blade (Marshall and Grant, 1995). Viscous effects can also substantially modify the vortex-blade interaction if the vorticity ejected from the blade boundary layer has sufficient time to interact strongly with the primary vortex (Kim and Komerath, 1995).

The important point to be made in the above discussion is that the maximum force induced by the vortex on the blade is strongly effected by details of the vortex structure and deformation during impact of the vortex on the blade. Research in this area, particularly with respect to acoustic aspects of vortex-blade interaction, typically employs some model of the vortex flow (such as that of a "frozen" vortex, inviscid flow, rapid distortion theory, circular core, etc.), but it is not at all clear that the choice of model does not have a significant effect on the predicted maximum blade force and sound generation.

On the other hand, direct computation of vortex impact on a blade in three dimensions from the Navier-Stokes equations is quite difficult and is not likely to be compatible with time requirements of the helicopter design process. Some form of modeling is clearly necessary if research in this area is to have any impact on helicopter design.

The approach taken in the present study is to first identify the physical characteristics of the flow during vortex impact on the blade in different parameter regimes, and then to evaluate possible computational and analytical models which can be used to describe aspects of the flow field. Section 2a gives an overview of the physical characteristics of the flow field during normal BVI as a function of the two parameters T/σ and $\Gamma/2\pi\sigma U$. A complementary summary was given by Kim and Komerath (1995), which describes various phenomena associated with rotor wake-cylinder interaction but does not span parameter space of T/σ and $\Gamma/2\pi\sigma U$. Also, Sheridan and Smith (1979) discuss the need for research in interactional aerodynamics in terms of helicopter flight performance. Section 2b considers the case in which the blade penetrates into the vortex core, and provides an assessment of the RDT approximation for this problem, which forms the basis of many acoustic analyses for normal vortex-blade interaction (Howe, 1989, Amiet et al., 1990). Conclusions and suggestions for future work are given in section 2c.

2a.) Regimes of normal blade-vortex interaction

Experiments have been performed in which a thin blade or a circular cylinder is moved through a nominally straight vortex with a non-zero axial flow. The vortex was formed using the vortex generator device described by Krishnamoorthy and Marshall (1994), using water as the working fluid. The diameter of the circular cylinder, the towing velocity of the blade or cylinder and the flow rate through the vortex generator device could all be varied, such that the parameters T/σ and $\Gamma/2\pi\sigma U$ could be adjusted from 0.7 - 17.6 and from 3.3 - 195, respectively. The axial velocity w in the vortex for all cases considered was such that the ratio $2\pi\sigma w/\Gamma$ was equal to about 0.15. The angle of attack, α, of the blade could also be adjusted from $-15°$ to $+15°$. Experimental results were obtained primarily by marking the intake vortex with red dye and the blade boundary layer by blue dye, and then photographing the resulting flow evolution. Measurements of vortex circulation and vorticity distribution were obtained both by photographing the motion of small (1-2 *mm*) immiscible dye globules immersed

in the boundary layer (Krishnamoorthy and Marshall, 1994) and by particle-image velocimetry.

(*i*) *Regimes of vortex-body interaction*

Three qualitatively different regimes of vortex-blade (or cylinder) interaction were identified. The first regime occurs for cases in which the parameter $\Gamma / 2\pi\sigma U$ is large (greater than about 20-30), so that the swirl velocity of the vortex is much larger than the convection speed of the vortex axis relative to the blade. In this strong-vortex regime, vorticity is ejected from the blade boundary layer while the vortex is still quite distant from the blade (5-10 core diameters or more). A sequence of pictures showing the evolution of the ejected vorticity for a case with $T / \sigma = 17.6$ and $\Gamma / 2\pi\sigma U = 40$ is given in figures 2a-d. The ejected vorticity rolls up into a vortex filament which is attached to the blade boundary layer at two points. This vortex filament wraps about the primary vortex, and the induced velocity from the secondary vortex loops cause formation of both axial waves (associated with variation of the core area) and helical waves (associated with displacement of the core axis) on the primary vortex. The wavelength of these waves on the primary vortex is of the same order as the distance between secondary vortex loops. These waves continue to grow in amplitude and decrease in wavelength, eventually resulting in complete disruption of the primary vortex, which may occur (for large $\Gamma / 2\pi\sigma U$) while the primary vortex is still separated from the blade by several core diameters.

The second regime occurs for weak vortices ($\Gamma / 2\pi\sigma U$ less than about 20) with thin blades (T / σ less than about 2). In this regime, the vorticity ejected from the blade boundary layer has little time to influence the primary vortex, and the blade penetrates into the vortex core with no significant deflection of the primary vortex axis. Once the blade penetration into the core occurs, computations for inviscid flow (see section 2b) indicate that the vorticity will accumulate in a thin "ribbon" of high-vorticity fluid which wraps about the blade leading edge. This vortex ribbon eventually decays due to viscous interaction with the underlying boundary layer on the blade, leading to connection of vorticity lines from the primary vortex with those in the blade boundary layer. Experiments with two color dyes indicate a strong entrainment of boundary layer fluid into the primary vortex core both above and below the blade.

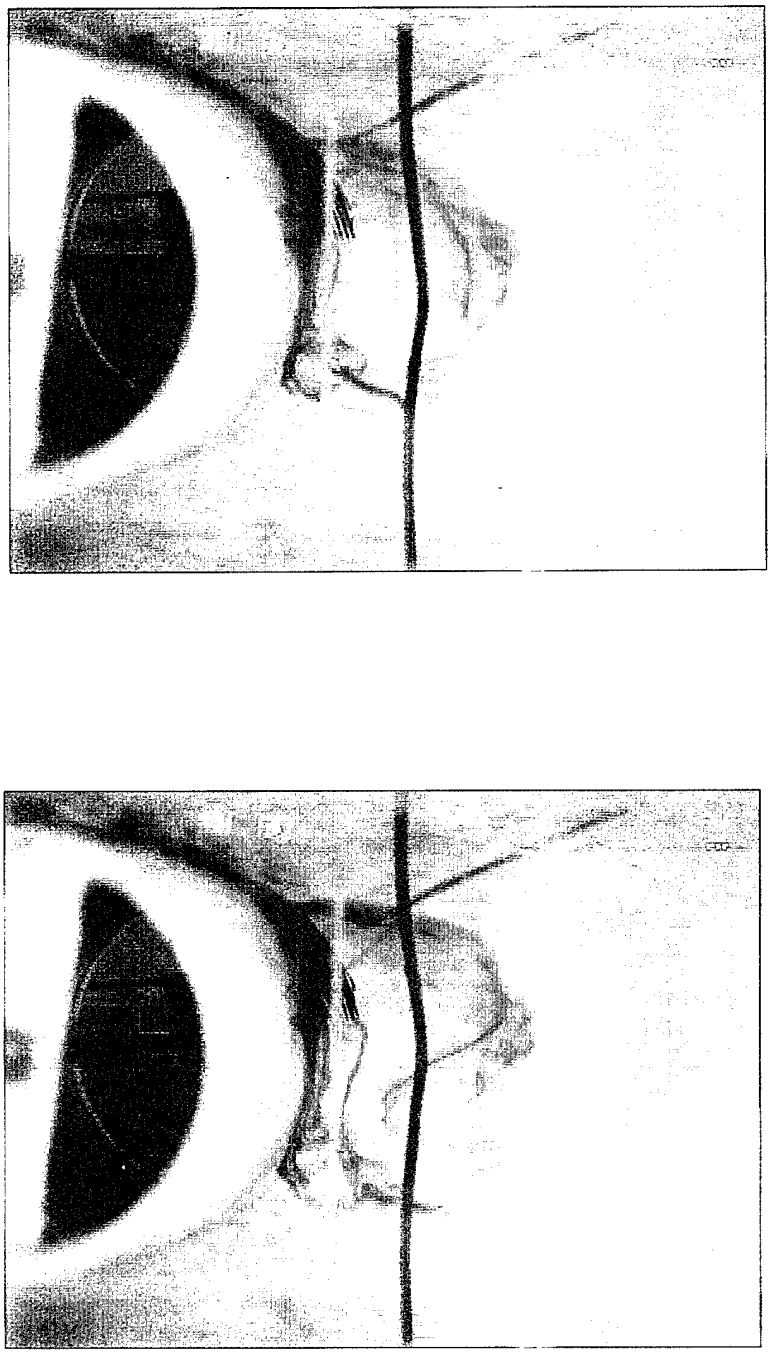

Fig. 2. Pictures showing secondary vortex wrapping about the primary vortex in the strong-vortex regime (regime 1). (a) Vorticity is ejected from blade boundary layer and pulled away from the blade by the primary vortex. (b) Secondary vortex filament completes one wrap about the primary vortex.

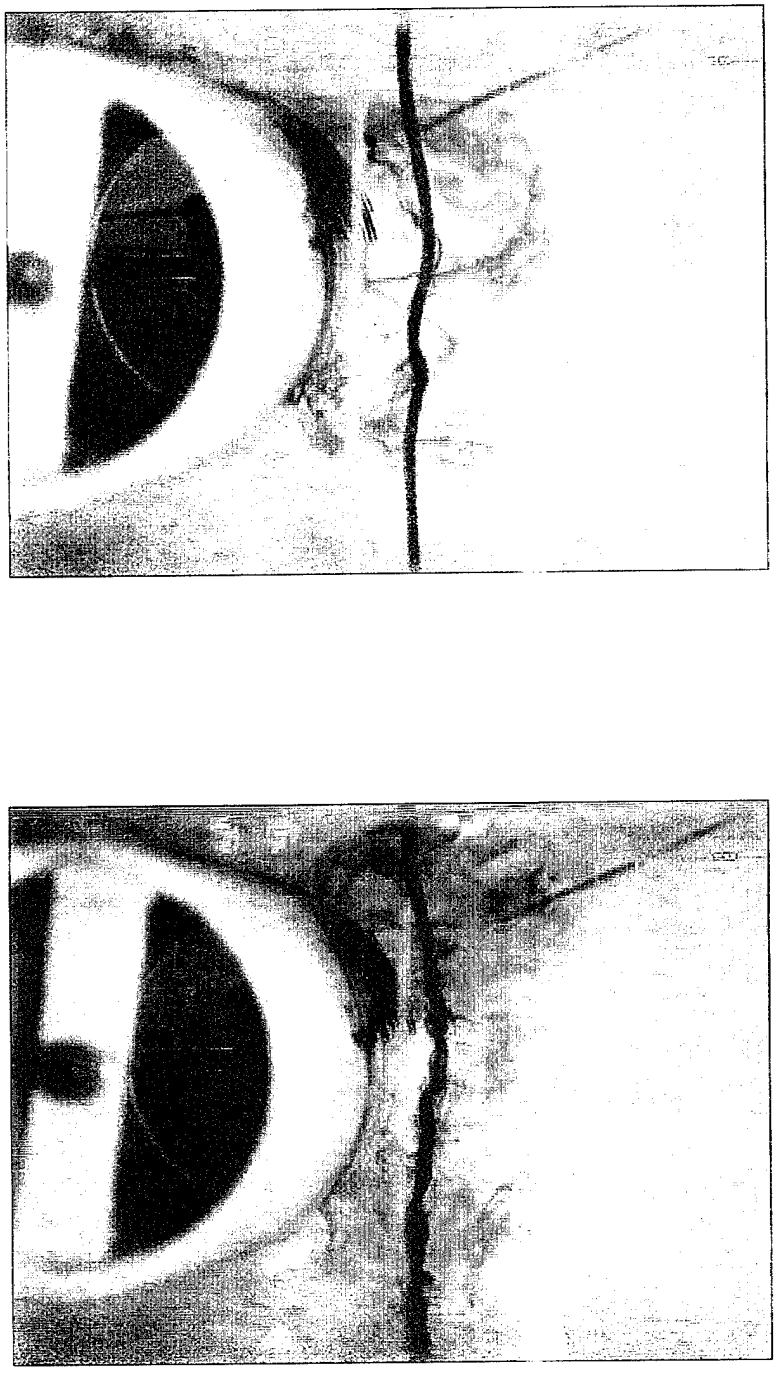

Fig. 2. Pictures showing secondary vortex wrapping about the primary vortex in the strong-vortex regime (regime 1). (c) Secondary vortex filament completes one and one-half wrap about primary vortex, and waves begin to form on the primary vortex. (d) Many waves form on primary vortex due to wrapped secondary vorticity, and the vortex disrupts completely shortly thereafter.

The third regime occurs for weak vortices ($\Gamma / 2\pi\sigma U$ less than about 10) but thick bodies (T / σ greater than about 5). In this regime, the vorticity ejected from the boundary layer again has little time to influence the primary vortex before it impacts on the body. However, for thick bodies (large T / σ), the vortex is observed both in experiments and in numerical computations (Affes and Conlisk, 1993, Marshall and Yalamanchili, 1994) to bend about the blade surface, as shown in figure 3 with $T / \sigma = 10$. For very small values of $\Gamma / 2\pi\sigma U$, substantial thinning of the vortex core occurs due to stretching by the blade (Marshall and Yalamanchili, 1994). After the vortex bends about the blade a certain amount (in a manner qualitatively similar to that predicted by vortex filament calculations), small helical waves develop on the vortex axis. These helical waves grow and eventually impinge on the boundary layer of the body, at which point the vortex rapidly disrupts into small scale turbulence. These helical waves, which lead to breakup of the vortex, may be caused either by inviscid instability of the vortex with its image over the body surface (Pedrizzetti, 1992) or by interaction with ejected vorticity from the body boundary layer.

In all three regimes of vortex-body interaction, a vortex breakdown forms on the vortex during impact with the blade and propagates up the vortex axis, opposite to the direction of the ambient axial flow in the core. The formation of the propagating vortex breakdown following cutting of the vortex is consistent with predictions of formation of a propagating vortex "shock" (i.e., a discontinuity in vortex core area) obtained using an extended vortex filament model which allows for variation in vortex core area (Marshall, 1994), as illustrated in figure 4. The measured propagation speed of the traveling vortex breakdown also agrees well with that predicted for the vortex "shock" in the filament model (Krishnamoorthy and Marshall, 1994). The traveling vortex breakdown was observed to be either of a spiral- or bubble-form (shown in figure 5a and b), which occurs for low and high values of $\Gamma / 2\pi\sigma U$, respectively. The dependence of breakdown form on $\Gamma / 2\pi\sigma U$, observed in the experiments, might be due to the fact that the breakdown develops when the vortex is still detached from the blade for large values of $\Gamma / 2\pi\sigma U$, while for small values of $\Gamma / 2\pi\sigma U$ it develops when the blade penetrates into the vortex core.

(*ii*) *Vortex-induced forces on the blade*

The vortex-induced forces on the blade during normal BVI result from three qualitatively different effects: (1) the reduction in surface pressure due to swirling motion

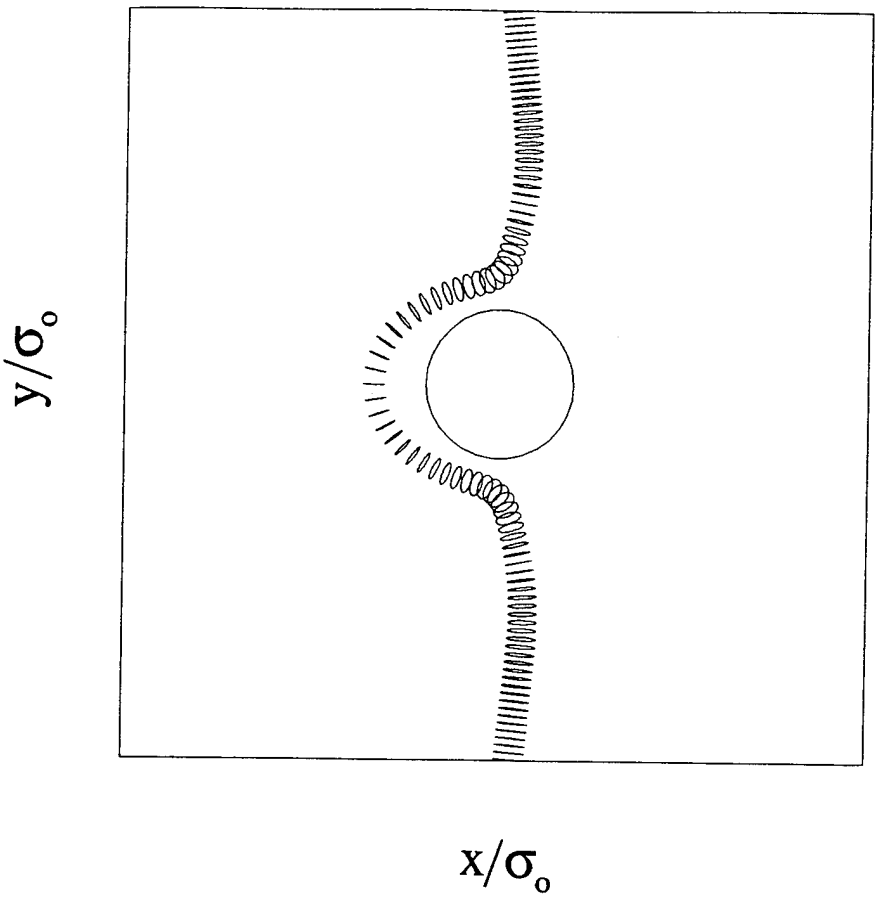

Fig. 3. Computation of a vortex bending about a circular cylinder in regime 3, with $T/\sigma = 10$ and $\Gamma/2\pi\sigma U = 2$.

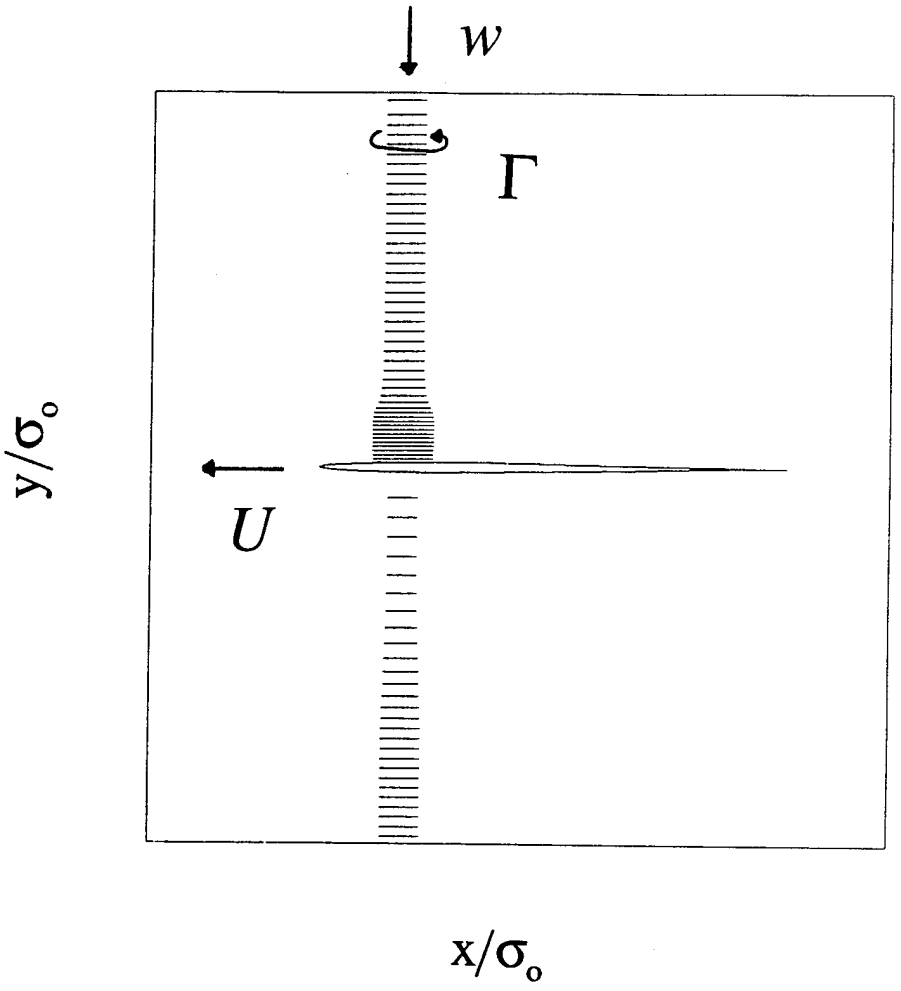

Fig. 4. Computation of vortex "shock" formed after cutting of vortex by blade, obtained using vortex filament theory with $T/\sigma = 1$, $2\pi\sigma w/\Gamma = -0.5$ and $\Gamma/2\pi\sigma U = 1$.

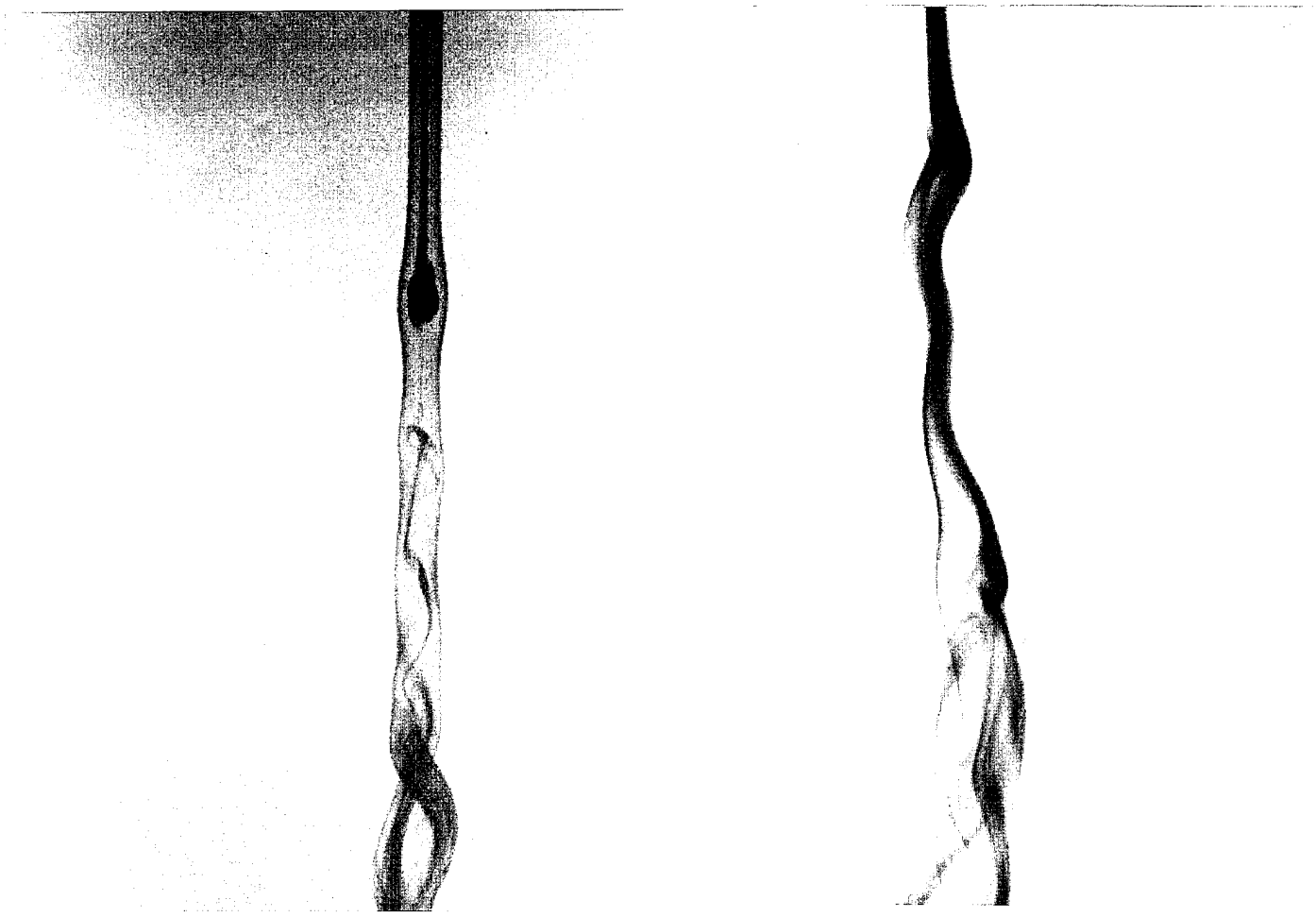

Fig. 5. Pictures of vortex breakdowns of the bubble and spiral types, both generated by cutting the vortex with a thin blade at zero angle of attack and propagating upward on the vortex axis. A bubble-type breakdown, which spirals into a double-helix downstream, is shown in (a) for the case $2\pi\sigma w / \Gamma = -0.16$ and $\Gamma / 2\pi\sigma U = 28$. A spiral-type breakdown is shown in (b) for the case $2\pi\sigma w / \Gamma = -0.26$ and $\Gamma / 2\pi\sigma U = 5.3$.

of the vortex, (2) blockage of the vortex axial flow as the blade cuts the vortex core, and (3) vorticity accumulation on the blade surface when the blade penetrates into the vortex core. The first and the third of these forces are oriented in the direction of relative motion between the blade and the vortex axis, and the second force is oriented in a direction tangent to the vortex axis.

The first of these forces can be accurately estimated using various vortex filament theories (Affes and Conlisk, 1993, Affes et al., 1993, Marshall and Yalamanchili, 1994), provided that the vortex is separated from the blade surface by several core diameters. When the separation distance between the vortex and the blade is on the order of a core diameter or less, deformation of the core and ejection of vorticity from the surface may significantly influence the blade force.

A model for the second force, due to blockage of axial flow, is given by Marshall (1994) and numerical calculations for this problem assuming axisymmetric inviscid flow have been performed by Lee et al. (1995), but the forces predicted by these studies have not yet been verified experimentally. While the predictions of the model of Marshall (1994) concerning formation and propagation of vortex breakdown on one side of the vortex after it has been cut by the blade agree well with experiments, this breakdown is observed in experiments to have a form which is sometimes far from axisymmetric (as shown in figure 5b). The assumption of axisymmetry for prediction of the axial flow blockage force thus requires further examination.

The third force mentioned above, which we will refer to simply as the blade penetration force, occurs only for the second regime of blade-vortex interaction, for which $T/\sigma \leq O(1)$ and $\Gamma/2\pi\sigma U$ is less than about 10. Since $\Gamma/2\pi\sigma U$ is relatively small in this regime, it is plausible that secondary vorticity ejection does not play a major role, so that the problem can be considered (at least initially) in terms of inviscid flow theory. The solution for the penetration force is greatly simplified by making use of rapid distortion theory (RDT), in which it is assumed that the vorticity field is convected only by the ambient potential flow about the blade. The use of RDT for calculation of blade penetration force was examined by comparison to direction computation by Marshall and Grant (1995), and the results of this investigation are reported in the next section.

2b.) Computations of blade penetration into a vortex core

Numerical calculations were performed for penetration of a NACA series 0016 airfoil, with equal span and chord lengths, into the core of a vortex ring. A uniform flow with speed U carries the vortex ring into the blade leading edge. All length and time scales are nondimensionalized by the chord length c and the ratio c/U, respectively. The core radius, σ, is 0.1 and the ring radius, R, is 0.5. The initial configuration for the calculations is shown in figure 6. A coordinate system is introduced such that the z-direction is along the blade leading edge, the x-direction is along the blade chord and the y-direction is normal to the symmetry plane of the blade. The blade is stationary and its leading edge is coincident with the line $x = y = 0$. The center of the ring is initially located at a distance of $x = -0.75$ upstream of the blade leading edge. Since the ring also propagates in the z-direction under its self-induced velocity field, an initial spanwise displacement of the ring is introduced such that the blade-vortex collision will occur close to the blade center ($z = 0$).

(*i*) *Numerical method*

The vortex evolution was computed by direct solution of the Euler equation for inviscid flows in vorticity-velocity space. The vorticity in the flow was marked using some number N control points. All of the calculations reported here were performed with both moderate resolution ($N = 3500$) and high resolution ($N = 10,500$), and the control points were three times as closely spaced on the side of the vortex which impacted on the blade. The control points were convected by the fluid flow, and the vorticity values on the control were evolved using the inviscid vorticity transport equation. The velocity field was obtained by solution of the Biot-Savart integral, using Gaussian blob functions to interpolate the vorticity field. Unlike traditional vortex blob methods, the amplitudes of the Gaussian blobs were fit to the vorticity values at the control points at every time step using a new iterative procedure, which is subjected to numerous validation tests by Marshall and Grant (1995). The no-penetration boundary condition on the blade surface was enforced using vorticity sheet panels on the surface (Hess and Smith, 1967), where the current computations utilize 900 quadrilateral panels to discretize the blade surface. The blade surface pressure was solved using an integral equation formulation of the pressure-Poisson equation (Uhlman, 1992).

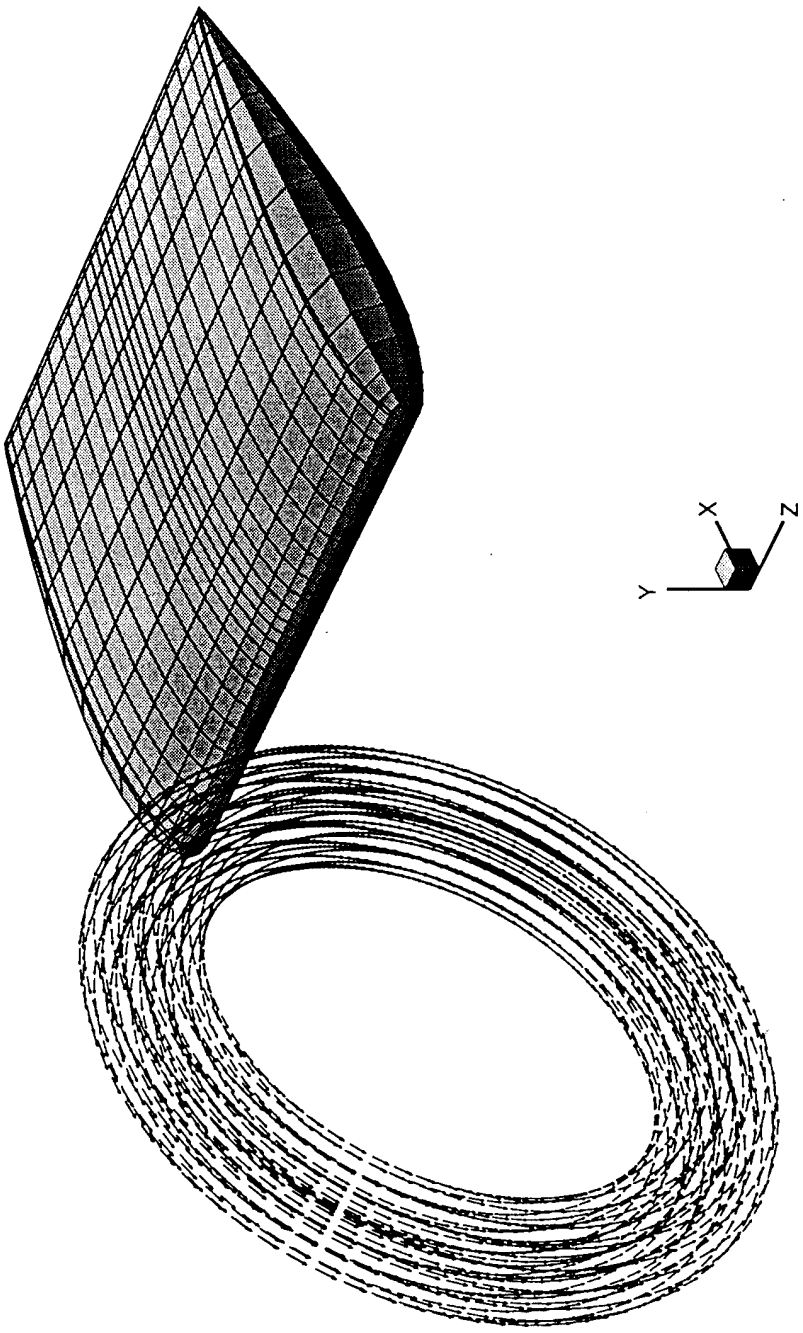

Fig. 6. Perspective view of the initial configuration for the computations of blade penetration into a vortex core.

Time advancement of the system was performed using the second-order predictor-corrector method with a time step of 0.005. The calculations were run for 70 time steps and were stopped at time $t = 0.35$, at which point the blade has completely penetrated through the ambient position of the vortex core. For the moderate resolution cases, runs were performed in which the time step was allowed to vary during the calculations between about 0.002 and 0.0001, with no noticeable difference in the computed results.

The radius of the vorticity elements was fit adaptively, by searching for nearest neighbors in three directions about each element, in order to ensure sufficient overlap between elements. The nominal initial element radius size was 0.04 for the moderate resolution cases and 0.03 for the high resolution cases. The element radius decreased for control points that approached the blade surface to about 0.03 - 0.025 for the moderate resolution cases and about 0.015 - 0.008 for the high resolution cases.

(*ii*) *Vorticity evolution*

In the present computations, the value of T / σ is fixed at 1.6, and computations are performed for three values of the parameter $\Gamma / 2\pi\sigma U$, given by 0.32, 0.79 and 1.6. All of these values lie in the second regime of vortex-blade interaction described in section 2a, so we would expect the blade to penetrate into the vortex core with little deflection of the vortex axis. One objective of these calculations is to compare results using the RDT approximation to those using the full inviscid theory. In RDT, the vorticity is assumed to be deformed by only the ambient potential flow about the blade, but the full velocity field (including that induced by the vortex and the vortex image) must be including in computing the blade surface pressure. In order for RDT to be valid, it is necessary for the time scale $t_d \approx T / U$ associated with deformation of the vorticity by the ambient potential flow to be small compared to the convection time $t_c \approx 2\pi\sigma^2 / \Gamma$ of the vortex-induced motion. This condition implies that the parameter $\varepsilon \equiv t_d / t_c \approx (\frac{T}{\sigma})(\frac{\Gamma}{2\pi\sigma U}) << 1$. The three cases considered in the paper, with $T / \sigma = 1.6$ and $\Gamma / 2\pi U\sigma = 0.32$, 0.79 and 1.6, correspond to ε values of 0.5, 1.3 and 2.5, respectively.

In order to evaluate the ability of the numerical method to resolve the vorticity deformation throughout the blade penetration process, the vortex circulation is calculated over a cross-section of the vortex core in the plane $y = 0$, which coincides with the plane

occupied by the blade chord. The circulation calculation is performed using two different methods. For the first method, the vortex-induced velocity tangent to a circuit surrounding the core, with a radius of three times the core radius, is integrated over the circuit to yield circulation. In the second method, the vorticity is interpolated using the vortex blob representation onto a uniform grid on the plane y=0, with 151 grid points on each side spanning the interval $(-0.5, 0.05)$ in x and $(-0.4, 0.4)$ in z, and the component of vorticity normal to this plane is integrated over area to obtain the circulation. A plot showing the results for these two methods of circulation measurement is given in figure 7 for high resolution runs with the three values of Γ considered in the paper. In this figure, square symbols denote results using the first method for circulation measurement and circular symbols denote results using the second method. The dashed lines correspond to the nominal values of circulation prescribed in the initial plane for the three cases. For all times shown, except for the last time considered for the case $\Gamma = 1$ (or $\Gamma / 2\pi U\sigma = 1.6$), the circulation obtained by either of these methods differs from the initial circulation by no more than 10%. In the last point shown in figure 7 for the case $\Gamma = 1$, the circulation obtained by the second method is 37% larger than the initial value, whereas that obtained by the first method is about 10% larger than the initial value. This point occurs at a time when the penetration of the blade through the ambient position of the vortex core is 87% complete. The differences between the two measures of circulation at this point could be indicative either of inadequacy of the element resolution during the later stages of the penetration (as will be discussed further presently) or of significant non-zero values of the vorticity divergence.

It is found for all three values of $\Gamma / 2\pi U\sigma$ considered that the vortex core exhibits relatively little response as it approaches the blade, aside from a slight flattening of the core, until the point where the blade leading edge actually begins to penetrate into the vortex core. If the vortex were to be convected with the uniform flow speed alone, the vortex would begin penetrating the blade at a dimensionless time of $t = 0.15$ and penetrate entirely through the blade by $t = 0.35$. A plot showing the vorticity field for the case $\Gamma / 2\pi\sigma U = 1.6$ for a moderate resolution run at dimensionless time $t = 0.30$, when the penetration process is about three-quarters complete, is given in figure 8. As would be expected from Helmholtz's observation that vortex lines and material lines coincide for an inviscid fluid, the computed vortex lines deform about the blade leading edge but are not cut by the blade. The highest vorticity magnitudes are observed in the computations to occur very close to the blade surface and to form a 'ribbon' of vorticity about the surface as the vortex is convected past the blade.

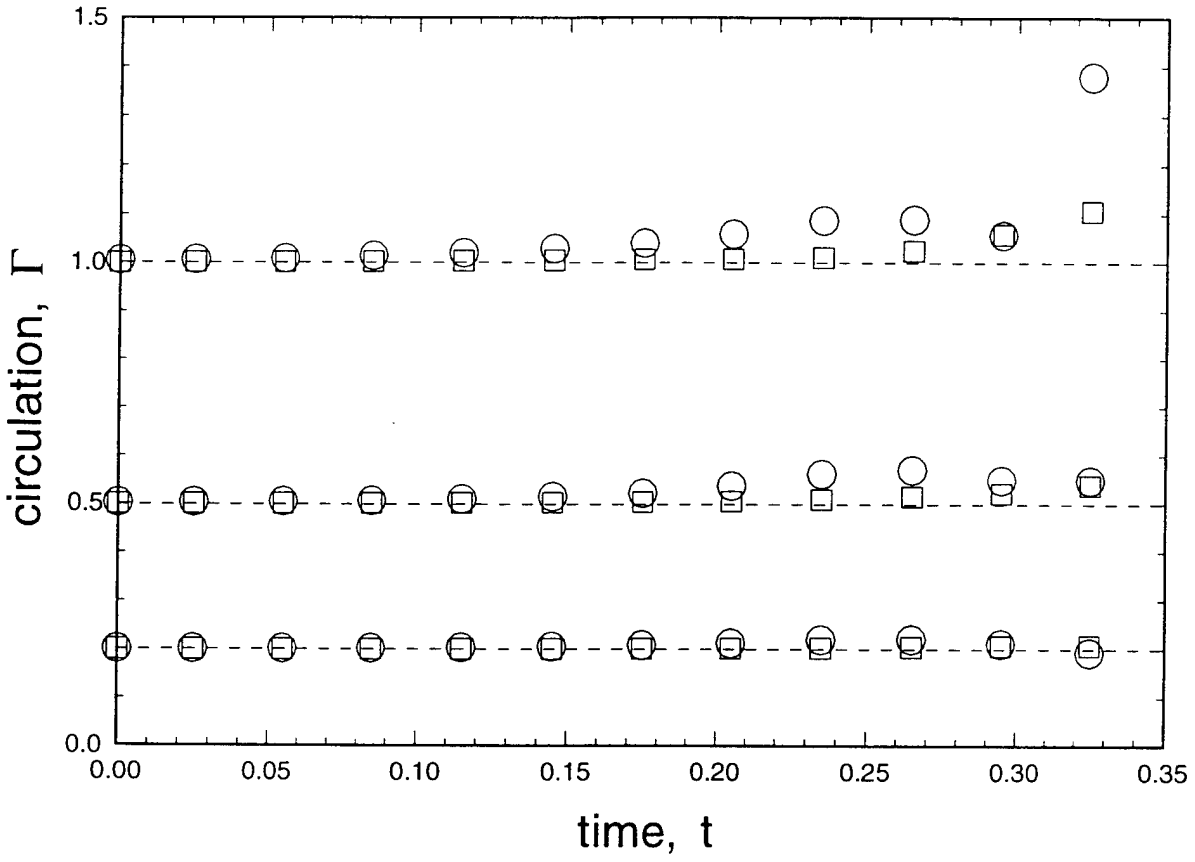

Fig. 7. Plot of the variation with time of the computed values of circulation in the $y = 0$ plane as the vortex is penetrated by the blade for the three nominal circulation values considered (shown by a dashed line). Points denoted by squares are computed using integration of velocity over a contour about the vortex core and points denoted by circles are computed by integration of vorticity over the cross-sectional area of the core.

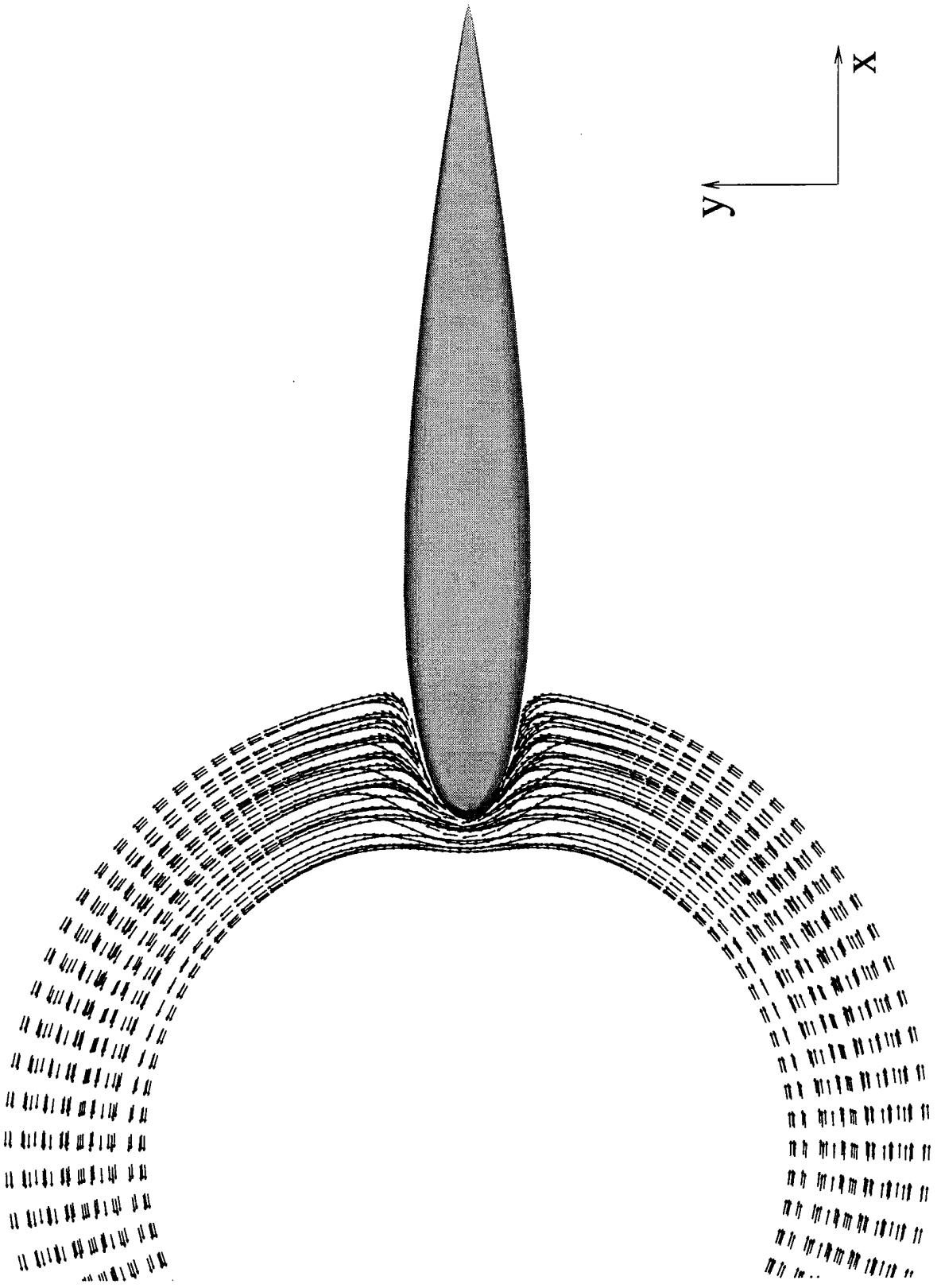

Fig. 8. Side view of the vorticity field for the case with $\Gamma / 2\pi\sigma U = 1.6$ at time t=0.23.

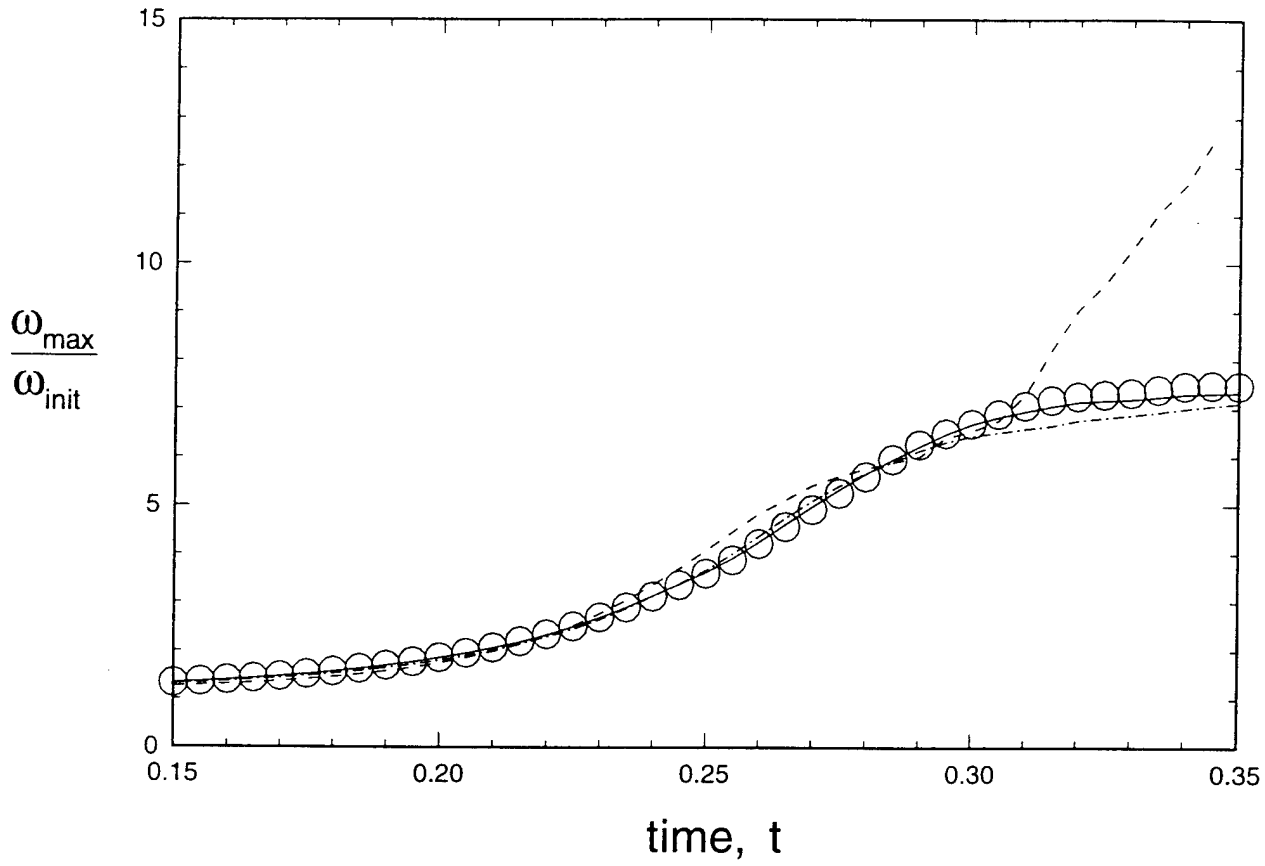

Fig. 9. Plot of average vorticity magnitude of the thirty control points with highest vorticity magnitude for cases with strong, moderate and weak vortices, with $\Gamma / 2\pi\sigma_0 U = 1.6$ (dashed curve), 0.79 (dashed-dotted curve) and 0.32 (solid curve), in comparison to RDT results (circles). The RDT results are the same for all values of $\Gamma / 2\pi\sigma_0 U$.

The average vorticity magnitude, ω_{max}, of the 30 control points with the highest vorticity magnitudes, divided by the initial maximum vorticity magnitude ω_{init}, is plotted in figure 9 versus time for all three values of the parameter $\Gamma / 2\pi\sigma_0 U$ with the high resolution runs. The time interval shown corresponds to that over which the vortex penetration occurs. The selection of 30 control points over which to average vorticity magnitude was found to give values fairly close to the peak vorticity values, while being somewhat smoother than averages with smaller number of points. Results for the full inviscid calculations are shown by solid, dashed-dotted, and dashed curves for cases with $\Gamma / 2\pi U\sigma_0 = 0.32$, 0.79 and 1.6, respectively. The results for $\omega_{max} / \omega_{init}$ obtained from the three RDT calculations were identical, since the vorticity was deformed only by the ambient potential flow. The RDT results are shown in figure 9 by circular symbols. The values of $\omega_{max} / \omega_{init}$ shown in figure 9 for the two full inviscid calculations with circulation of $\Gamma = 0.2$ and 0.5 are very close for the RDT results. In the case with $\Gamma = 1$, the value of this ratio deviates from that for the RDT calculation at a time of about 0.31, after about 80% of the blade penetration is complete. The deviation of $\omega_{max} / \omega_{init}$ for the strong vortex case from that obtained for weaker vortices could be caused by stretching of the vorticity by interaction with its image in the blade, which would not be as prevalent for cases with weaker vortices, or by the numerical difficulties encountered at the end of this run, as noted in the discussion of figure 7. It is also noted that the leveling off of the maximum vorticity values in figure 9 after the penetration is about 75% complete (for $t > 0.30$) is due to the limitation on the ability of the vorticity blobs to resolve the very thin vortex ribbon about the blade surface during the latter part of the runs.

(*iii*) *Blade surface pressure and force*

A contour plot of the change in blade surface pressure from its value without the vortex present is given in figure 10 for a moderate resolution run with $\Gamma / 2\pi\sigma_0 U = 1.6$. The plot is made at $t = 0.26$, at which time the vortex penetration is roughly half completed, and shows the vorticity vector only at every fourth control point in order to indicate the general location of the vortex. The pressure signature on the blade surface is dominated by a 'V' of low pressure, in the center of which (at the blade leading edge) there is a patch of high pressure. The low pressure patches on the top and bottom of the blade are due to the low pressure within the vortex core, and the low and high pressure regions along the blade leading edge are caused by the induced velocity from the vortex as it impinges on the blade. The "waviness" of the element arrows at the top and bottom

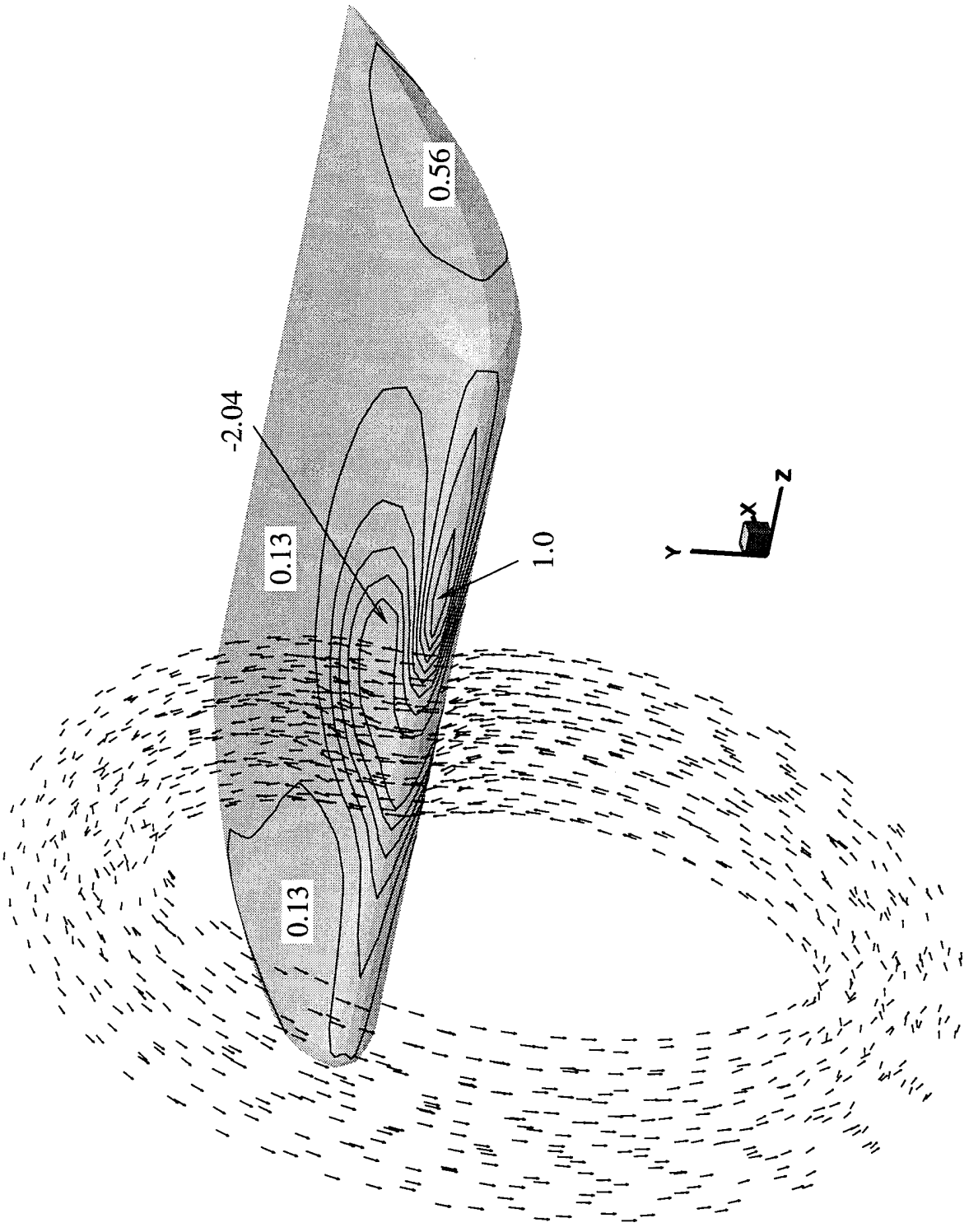

Fig. 10. Contour plot of the pressure change on the blade surface due to the vortex for a case with $\Gamma / 2\pi\sigma_0 U = 1.6$ and at time $t = 0.26$. One-fourth of the vorticity control point positions are shown to indicate the position of the vortex.

of the ring is an optical effect due to looking along the core axis (such waviness is not apparent in the side view in figure 8).

The pressure signature for the weak vortex case appears similar to that shown in figure 10, except that high pressure regions are also found on the top and bottom of the blade on the opposite side (i.e., for opposite values of z) of that on which the low pressure regions occur. The general appearance of the pressure signature for weak vortices is that of two interlocking V's of high and low pressure.

A plot of time variation of the pressure coefficient $C_{p,\min}$ associated with the minimum surface pressure on the blade, defined by

$$C_{p,\min} = \frac{p_0 - p_{\min}}{\frac{1}{2}\rho\Gamma^2/\sigma_0^2}, \tag{1}$$

is given in figure 11 for the high resolution calculations with three different values of ring circulation. Results of the full inviscid calculations are shown by continuous curves and results for RDT calculations are shown by symbols. In the implementation of RDT in our computations, the vorticity is convected with only the ambient potential flow but the full velocity is used for evaluation of pressure. It is found that if only the ambient potential flow is used in the pressure calculation, the computed unsteady drag force on the blade is much too small. In an analytical study using RDT together with the thin airfoil approximation, Howe (1989) also found that the spanwise velocity components, induced by the vortex and its image over the blade surface, play an important role in determination of the unsteady blade force.

The results of the full inviscid computations for the lower two circulation values compare closely with the RDT runs, but the results for the highest circulation value oscillate about the RDT results. The pressure field for runs with strong vortices is dominated by the vortex-induced velocity and would therefore be expected to vary approximately in proportion to Γ^2. For much weaker vortices, the pressure field is influenced more by the perturbation which the vortex causes to the ambient velocity field, and would therefore vary approximately in proportion to $U\Gamma$. Since the three cases plotted in figure 11 include vortices ranging from fairly weak to fairly strong (compared to the free stream flow), the minimum pressure coefficient is lower for cases with stronger vortices.

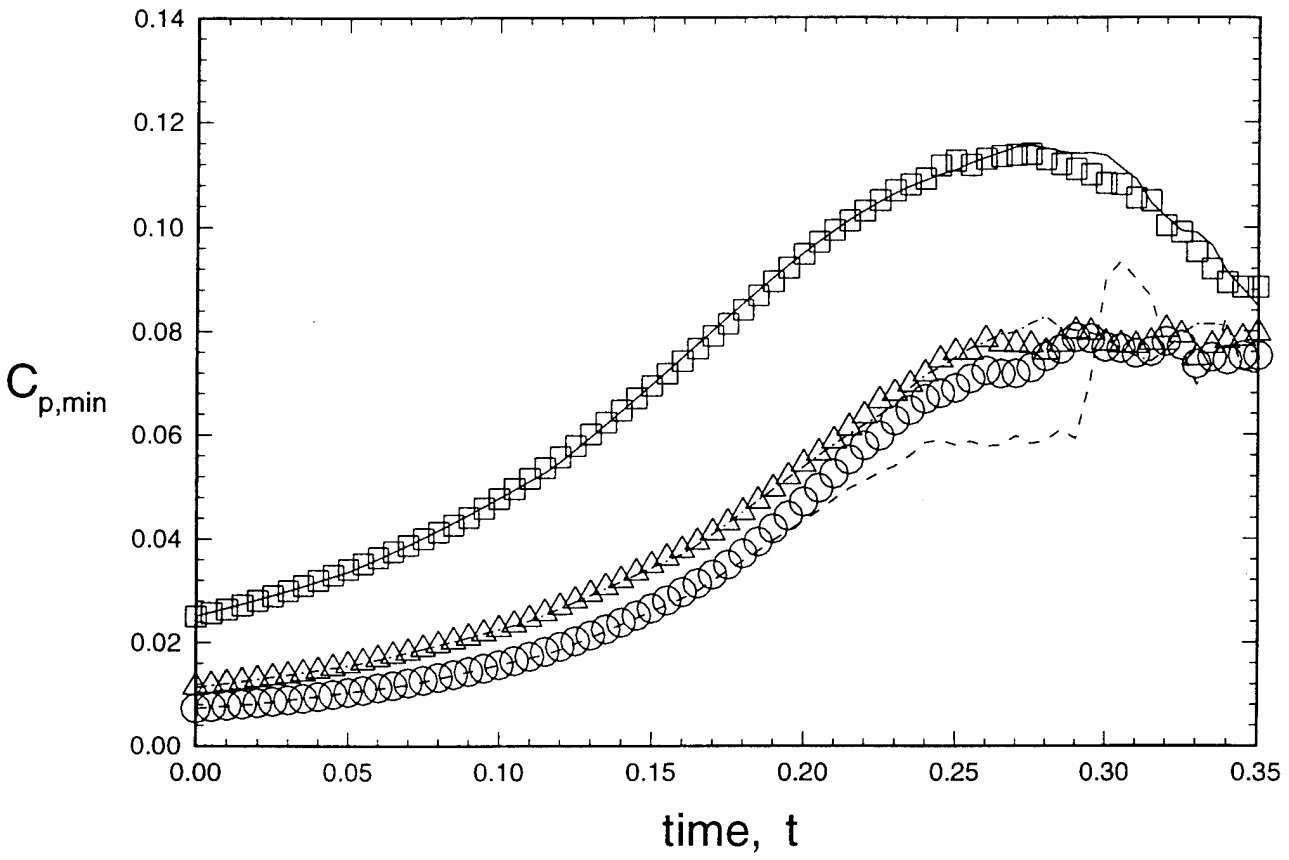

Fig. 11. Plot of variation of the minimum value of the blade surface pressure coefficient $C_{p,\min}$ with time for cases with strong, moderate and weak vortices, $\Gamma / 2\pi\sigma_0 U$ = 1.6 (dashed curve), 0.79 (dashed-dotted curve) and 0.32 (solid curve), in comparison to RDT results, denoted by circles, triangles and squares, respectively.

The computational results for vortex-induced drag D on the blade are plotted in figure 12 for high-resolution runs in terms of the drag coefficient C_D, defined by

$$C_D = \frac{-D}{\frac{1}{2}\rho\Gamma^2} \,. \tag{2}$$

The computed results for C_D from the RDT calculations are found to be identical (to within plotting accuracy) for all three values of circulation considered, even though the pressure results shown in figure 11 are quite different. Furthermore, the results of the full inviscid calculations are found to coincide very closely to the RDT results for $t < 0.29$ for all three circulation values considered. For $t > 0.29$, the full inviscid calculations for the cases with $\Gamma = 0.5$ and 1.0 (corresponding to $\varepsilon = 0.79$ and 1.6, respectively) give somewhat larger values for C_D than predicted by RDT. Since both the maximum vorticity values and the minimum pressure values for the case with $\Gamma = 0.5$ agree closely with the RDT results during this time period (as shown in figures 9 and 11), it seems unlikely that the observed differences in drag coefficient for this case are due to numerical resolution difficulties (which would tend to have most effect on points with largest vorticity values in the ribbon about the blade surface). These differences in C_D with the RDT predictions seem to arise from breakdown of the RDT assumption as the parameter ε approaches and exceeds unity, resulting in differences in large-scale deformation of the vortex between the RDT and full inviscid calculations.

The variation of blade penetration force with Γ^2, which is evident from figure 12 during the first 70-75% of the penetration process, can be explained by recalling the identity obtained by Howe (1989, Eq. (A.4)), which gives the drag force due to an inviscid vorticity field external to a stationary body, with constant uniform flow at infinity, by the integral

$$D = \rho \int_V \vec{\nabla}\phi \cdot (\vec{\omega} \times \vec{\mathbf{u}}_{vort}) \, dv \,. \tag{3}$$

Here ϕ is the velocity potential due to a uniform potential flow (with unity flow speed at infinity) past the body and $\vec{\mathbf{u}}_{vort}$ is the velocity induced by the vortex and its image. If the deformation of the vorticity field were due primarily to the ambient potential flow past the body, as assumed in RDT, then both $\vec{\omega}$ and $\vec{\mathbf{u}}_{vort}$ would be proportional to Γ, so that D

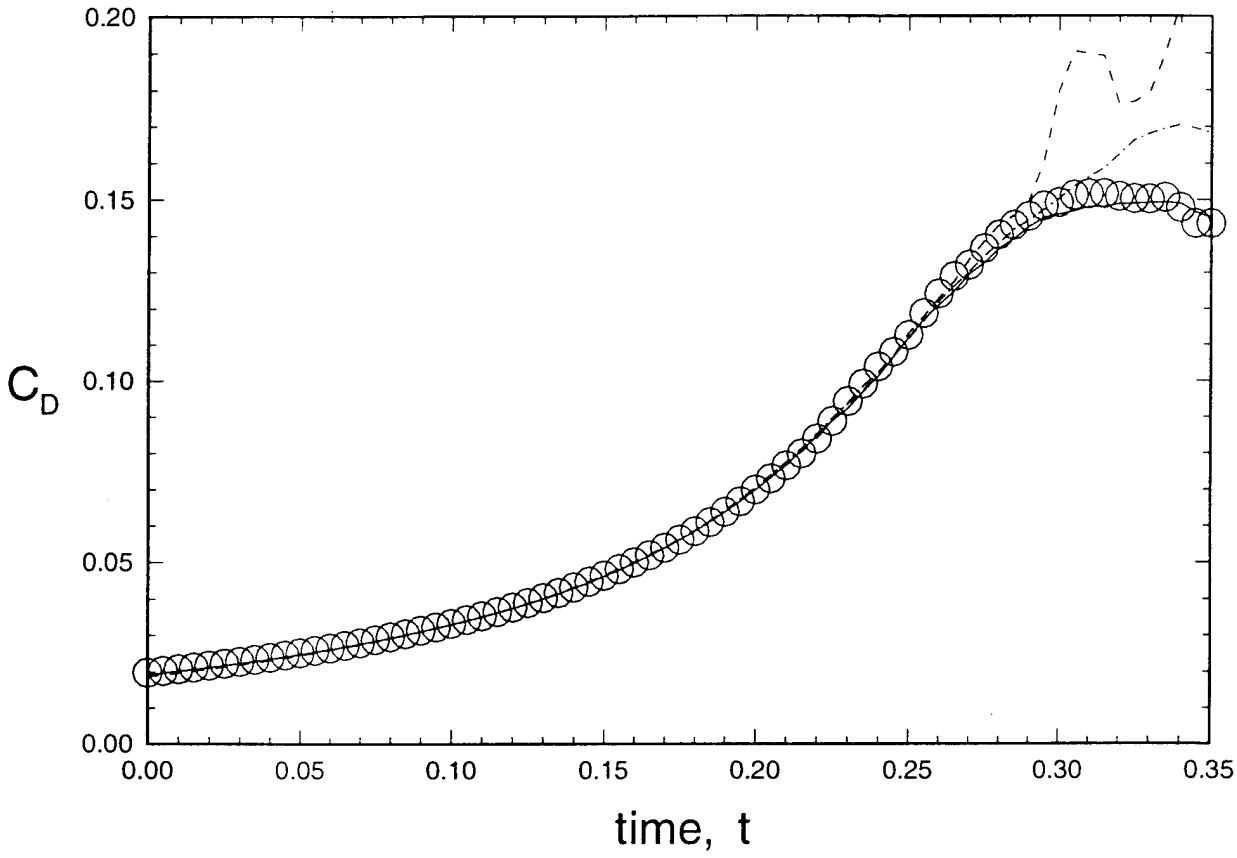

Fig. 12. Plot of variation of the drag coefficient C_D with time for cases with strong, moderate and weak vortices, $\Gamma / 2\pi\sigma_0 U = 1.6$ (dashed curve), 0.79 (dashed-dotted curve) and 0.32 (solid curve), in comparison with RDT results (circles). The RDT results are the same for all values of $\Gamma / 2\pi\sigma_0 U$.

would be proportional to Γ^2 and (3) would yield the result that the value of C_D is independent of Γ (as our computed results with RDT show). On the other hand, if the vortex were sufficiently strong that the vortex-induced or image velocity contributed significantly to deformation of the vorticity field, then the vortex stretching term in the vorticity transport equation would exhibit both terms which are linear and quadratic in Γ, and (3) would indicate that the drag will no longer be proportional to Γ^2.

(*iv*) *Comparison of different vortex-induced forces on the blade*

It may be of interest at this point to compare the magnitude of the blade penetration force with that of other forces present in typical normal BVI applications. For instance, for non-zero angles of attack α, the normal BVI force is calculated in Marshall and Yalamanchili (1994) prior to impact of the blade on the vortex using a vortex filament model. This force is found to increase with increasing values of α and T / σ_0. For instance, in figure 10 of Marshall and Yalamanchili (1994) (which is for a case with $T/\sigma_0 = 5$ and attack angles of $\alpha = 0°$ and 15°), the peak drag coefficients are found to be about $C_D = 0.3$ and 0.5, respectively. In comparison, if we assume that the blade penetration force increases in proportion to the ratio T / σ_0 (for sufficiently small values of this ratio) and vanishes for $T / \sigma_0 = 0$ (both of which are consistent with the result in Eq. (3.20) of Howe, 1989), the peak value from figure 12 can be extrapolated for a case with $T/\sigma_0 = 5$ to give a peak value of approximately $C_D \cong 0.5$. For cases with $T / \sigma_0 = O(1)$, the blade penetration force thus seems to make a significant contribution to the total vortex-induced force on the blade.

3. Conclusions and Future Work

Three regimes of vortex-blade interaction have been experimentally identified, based on the values of the two dimensionless parameters T / σ and $\Gamma / 2\pi\sigma U$. For large values of $\Gamma / 2\pi\sigma U$, the interaction is controlled by vorticity eruption from the blade boundary layer, followed by wrapping of the secondary vorticity about the primary vortex and subsequent breakup of the primary vortex. Calculations of vortex-induced separation from a circular cylinder have been recently been reported by Affes et al. (1994) based on boundary layer theory. However, there is very little literature pertaining to the problem of wrapping of secondary vorticity about the primary vortex and the observed primary vortex breakup in this regime.

As $\Gamma / 2\pi\sigma U$ decreases below about 10-20, the secondary vorticity plays a progressively smaller role in the vortex-blade interaction. For the case of small $\Gamma / 2\pi\sigma U$ and T / σ much greater than O(1), the vortex is observed to bend about the blade (or cylinder) much as is predicted by the vortex filament theory. When vortex breakup finally does occur in this regime, it is preceded by formation of short helical waves on the vortex core, which grow and impinge on the body surface. If these waves are due to inviscid instability of the primary vortex with its image, they should be observed in the vortex filament predictions provided that the spatial resolution is sufficient and that initial small perturbations over a spectrum of wavelengths are introduced on the vortex core. Alternatively, the waves could be due to interaction with shed vorticity from the blade boundary layer as the primary vortex is bent about the body. Based on estimates from linear stability theory and flow visualization, it seems that both of these effects could be significant.

For the case of small $\Gamma / 2\pi\sigma U$ and T / σ of O(1) or smaller, the blade penetrates into the vortex core. The deformation of the vorticity field during blade penetration was examined in detail, for an inviscid flow, by Marshall and Grant (1995). The vorticity is observed to accumulate into a thin vorticity "ribbon" which wraps about the blade surface. Comparison of results of direct computations from the Euler equations and calculations using the RDT approximation indicates that RDT is valid for this problem for $(\Gamma / 2\pi\sigma U)(T / \sigma)$ less than about unity. For values T / σ much less than unity, the blade penetration force would be small compared to other forces present. Problems which have not been resolved for this regime include the decay of the vorticity "ribbon" due to viscous effects and the force exerted by blockage of the axial flow within the vortex as it is cut by the blade.

LIST OF PUBLICATIONS AND TECHNICAL REPORTS

The following publications have resulted from the research supported through this project.

A. Journal Papers, In Press or Published

1. Marshall, J.S. and Grant, J.R., "Penetration of a Blade Into a Vortex Core: Vorticity Response and Unsteady Blade Forces," *Journal of Fluid Mechanics* (in press).

2. Krishnamoorthy, S. and Marshall, J.S., "An Experimental Investigation of 'Vortex Shocks'," *Physics of Fluids*, Vol. 6, No. 11, 1994, pp. 3737-3741.

3. Marshall, J.S., "Vortex Cutting by a Blade. Part I. General Theory and a Simple Solution," *AIAA Journal*, Vol. 32, No. 6, 1994, pp. 1145-1150.

4. Marshall, J.S., and Yalamanchili, R., "Vortex Cutting by a Blade. Part II. Computations of Vortex Response," *AIAA Journal*, Vol. 32, No. 7, 1994, pp. 1428-1436.

5. Marshall, J.S., and Grant, J.R., "Evolution and Break-Up of Vortex Rings in Straining and Shearing Flows," *Journal of Fluid Mechanics*, Vol. 273, 1994, pp. 285-312.

B. Journal Papers, Submitted or In Preparation

1. Marshall, J.S. and Grant, J.R., "A Method for Determining the Velocity Induced By Highly Anisotropic Vorticity Blobs," submitted to the *J. Computational Physics.*

2. Marshall, J.S., Grant, J.R. and Chen, H., "A Lagrangian Vorticity Collocation Method for Solution of Viscous Fluid Flows Past Immersed Bodies," to be submitted to the *J. Computational Physics.*

C. Conference Papers

1. Marshall, J.S. and Grant, J.R., "A Lagrangian Collocation Method for Vorticity Transport in Viscous Fluid Flows," Proc. of the Forum on the Appl. of Vortex Methods to Engineering Problems, Sandia Natl Labs., Albuquerque, New Mexico, Feb. 22-24, 1995.

2. Marshall, J.S. and Grant, J.R., "Computation and Modeling of Blade Penetration Into a Vortex in an Inviscid Fluid," 26th AIAA Fluid Dynamics Conference, San Diego, June 1995, AIAA paper 95-2239 (invited paper).

D. Technical Reports

1. Marshall, J.S., "The Fluid Mechanics of Vortex Cutting By a Blade," Report submitted to A.R.O. during Sept., 1993.

E. Theses and Dissertations

1. Krishnamoorthy, S., "An experimental study of vortex response during cutting by a blade or cylinder," M.S. thesis, Florida Atlantic University, Dept. Ocean Engineering, Dec. 1993.

2. Yalamanchili, R., "Computations of normal vortex interaction with blades and circular cylinders," M.S. thesis, Florida Atlantic University, Dept. Ocean Engineering, Dec. 1993.

LIST OF PARTICIPATING SCIENTIFIC PERSONNEL

1. J.S. Marshall, Principal Investigator

2. S. Krishnamoorthy
   M.S. degree received from Florida Atlantic University, Dec. 1993
   Currently Ph.D. candidate at The University of Iowa

3. R. Yalamanchili
   M.S. degree received from Florida Atlantic University, Dec. 1993

4. H. Chen
   Currently Ph.D. candidate at The University of Iowa

REPORT OF INVENTIONS

No inventions were made in the course of this project.

BIBLIOGRAPHY

1. Affes, H. and Conlisk, A.T., "Model for Rotor Tip Vortex-Airframe Interaction. Part 1: Theory," *AIAA J.*, Vol. 31, No. 12, 1993, pp. 2263-2273.

2. Affes, H., Conlisk, A.T., Kim, J.M. and Komerath, N.M., "Model for Rotor Tip Vortex-Airframe Interaction. Part 2: Comparison with Experiment," *AIAA J.*, Vol. 31, No. 12, 1993, pp. 2274-2282.

3. Affes, H., Xiao, Z. and Conlisk, A.T., "The Boundary Layer Flow Due to a Vortex Approaching a Cylinder," *J. Fluid Mech.*, Vol. 275, 1994, pp. 33-57.

4. Amiet, R.K., Simonich, J.C. and Schlinker, R.H., "Rotor Noise Due to Atmospheric Turbulence Ingestion. Part II: Aeroacoustic Results," *J. Aircraft*, Vol. 27, No. 1 1990, pp. 15-22.

5. Kim, J.M. and Komerath, N.M., "Summary of the Interaction of a Rotor Wake with a Circular Cylinder," AIAA J., Vol. 33, No. 3, 1995, pp. 470-478.

6. Krishnamoorthy, S. and Marshall, J.S., "An Experimental Investigation of 'Vortex Shocks'," *Phys. Fluids*, Vol. 6, No. 11, 1994, pp. 3737-3741.

7. Hess, J. and Smith, A., "Calculation of Potential Flows About Arbitrary Bodies," *Prog. Aeronaut. Sci.*, Vol. 8, 1967, pp. 1-138.

8. Howe, M.S., "On Unsteady Surface Forces, and Sound Produced by the Normal Chopping of a Rectilinear Vortex," *J. Fluid Mech.*, Vol. 206, 1989. pp. 131-153.

9. Lee, J., Xiao, Z., Burggraf, O.R., Conlisk, A.T. and Komerath, N.M., "An Inviscid Analysis of Vortex-Surface Collisions," AIAA Paper 95-2237, June 19-22, 1995

10. Leverton, J.W., Pollard, J.S. and Wills, C.R., "Main Rotor Wake/Tail Rotor Interaction," *Vertica*, Vol. 1, 1977, pp. 213-221.

11. Marshall, J.S., "The Fluid Mechanics of Vortex Cutting By a Blade," Report submitted to ARO during Sept., 1993.

12. Marshall, J.S., "Vortex Cutting by a Blade. Part I. General Theory and a Simple Solution," *AIAA J.*, Vol. 32, No. 6, 1994, pp. 1145-1150.

13. Marshall, J.S., and Yalamanchili, R., "Vortex Cutting by a Blade. Part II. Computations of Vortex Response," *AIAA J.*, Vol. 32, No. 7, 1994, pp. 1428-1436.

14. Marshall, J.S. and Grant, J.R., "Penetration of a Blade Into a Vortex Core: Vorticity Response and Unsteady Blade Forces," *J. Fluid Mech.* (in press).

15. Pedrizzetti, G., "Close Interaction Between a Vortex Filament and a Rigid Sphere," *J. Fluid Mech.*, Vol. 245, 1992, pp. 701-722.

16. Saffman, P.G. and Tanveer, S., "The Touching Pair of Equal and Opposite Uniform Vortices," *Phys. Fluids*, Vol. 25, No. 11, 1982, pp. 1929-1930.

17. Sheridan, P.F. and Smith, R.P., "Interactional Aerodynamics - A New Challenge to Helicopter Technology," Proc. 35th Ann. Nat. Forum of the American Helicopter Society, Wash. D.C., May 1979.

18. Uhlman, J.S., "An integral equation formulation of the equations of motion of an incompressible fluid," Technical Report NUWC-NPT 10086, 1992.